Numerically obtained vortices in granular media

2 authors:

Dimitrios Kolymbas
University of Innsbruck
57 PUBLICATIONS   **1,825** CITATIONS

SEE PROFILE

Iman Bathaeian
ILF Consulting Engineers Austria GmbH
9 PUBLICATIONS   **30** CITATIONS

SEE PROFILE

Some of the authors of this publication are also working on these related projects:

Project   Tunneling View project

Project   A Meshfree Numerical Approach for Soils at Rest and in Flow View project

Numerically obtained vortices in granular media

Dimitrios Kolymbas[1] | Iman Bathaeian*[1,2]

[1]Unit of Geotechnical and Tunnel
Engineering, University of Innsbruck,
Innsbruck, Austria
[2]Geotechnical Department, ILF Consulting
Engineers, Innsbruck, Austria

Correspondence
*Iman Bathaeian, Email:
Iman.Bathaeian@ilf.com

Summary

With our meshfree numerical code SPARC, which is based on strong solutions of the
equations of equilibrium, we were able to derive vortex patterns ("turbulence") in
deformations hitherto believed to be homogeneous. The formation of such vortices
demonstrates the non-uniqueness of the corresponding boundary value problem. We
present some evidence that such vortices can be related with ptygmatic folds, that
are observed in rock.

KEYWORDS:
meshfree method, SPARC, vortex (turbulence), second order work, ptygmatic folds

1 | INTRODUCTION

In this paper we consider vortices that appear in the course of deformation of soil. To denote this vorticity we use the word
'turbulence', which is established in fluid mechanics. Of course, in fluids turbulence has to do with a surplus of kinetic energy,
whereas the motions of sand considered here are slow. Thus, turbulence in granulates is not exactly the same as turbulence in
fluids, but in both cases the appearance of vortices is predominant. Vortices can be observed in laboratory tests with Digital
Image Correlation. The vortices appear in the fields of velocity fluctuations $\mathbf{v}' = \mathbf{v} - \bar{\mathbf{v}}$. Abedi et al.[1] have observed vortices in
a biaxial test in softening regime and critical state. Richefeu et al.[2] show velocity fluctuations in a so-called $1\,\gamma\,2\,\varepsilon$ - apparatus,
which allows the application of shear (γ) and rectilinear extension (ε). Admittedly, DEM simulations do not necessarily mirror
the reality. However, they often reveal realistic pictures of the deformation. There are several reports on vortices in the fluctuation
velocity fields, obtained with DEM, such as the ones reproduced by Thornton and Zhang[3] in simple shear test, by Kozicki
et al.[4] in direct shear test, by O'Donovan et al.[5] in triaxial tests and by Peters and Walizer[6] in biaxial tests. In this paper we
report on numerically obtained vortices that appear in the course of element tests. Such tests are commonly believed to exhibit
only homogeneous deformations. Therefore, we first consider whether uniqueness (of homogeneous solution in element tests)
is really necessary.

2 | ELEMENT TESTS AND THEIR CONTROLLABILITY

"Element tests" are by definition tests with spatially constant stress and deformation. The latter means that the displacements
(or velocities) depend in a linear (or affine) way on the spatial coordinates $\mathbf{x}$. Therefore, an inhomogeneous displacement field
is also called a non-affine displacement field.
In order to deduce stress-strain relations from laboratory tests, they must be element tests. Otherwise, it is not possible to infer
the stress and strain from the measured forces and displacements, respectively. In this respect the question arises how to enforce
homogeneous deformation of a sample or, in other words, how to control the sample deformation by applying tractions and
displacements to its boundary. For an element test to be "controllable" at a particular stress state $\mathbf{T}$, one must,

1. prescribe

(a) the boundary displacements (or velocities) as linearly dependent on the boundary coordinates $\mathbf{x}_B$: $\mathbf{v}_B = \mathbf{A}\mathbf{x}_B$, with $\mathbf{A}$ = const, in one part of the boundary, and

(b) the boundary tractions $\mathbf{t} = \mathbf{T}_B\mathbf{n}_B$ in the complementary part of the boundary.

2. Inequality 4 must be fulfilled.

In the words of Revuzhenko[7], the fulfillment of an affine velocity distribution $\mathbf{v} = \mathbf{A}\mathbf{x}$ on the boundary of an element test implies its fulfillment also in the interior of the sample provided (i) that mass forces are absent and (ii) response is unique.

It is common in soil mechanics to assume that triaxial tests with smooth end plates are element tests at the beginning of the deformation, until an inhomogeneous mode of deformation (usually a localized shear band) sets in at a certain bifurcation point. In particular, oedometric tests with smooth side walls and end plates are considered as unconditionally controllable, i.e. having homogeneous deformation.

However, smooth side walls and end plates impose the normal velocity but *not* the tangential velocity of the boundary. Thus, the boundary velocities are *not* fully prescribed. Therefore, *neither oedometric nor triaxial tests are necessarily related with a unique deformation of a soil sample!* Note that this statement refers to materials which are not linear-elastic and implies that inhomogeneous (non-affine) deformations can appear even at the very beginning of the test,[8,9] and they can be manifested with vortices. There is plenty of evidence of vortices in granular media, observed with DIC (digital image correlation) and also with DEM simulations. The special case of shear bands can be interpreted as so-called vortex sheets, i.e. as planar arrays of vortices. In the laboratory, rigid confinements of a sample are either smooth or, in the ideal case, absolutely rough. In the first case the boundary displacements are not fully prescribed, in the second case no deformation is allowed adjacent to the boundary. In either cases, rigid confinements are inappropriate for element tests!

3 | UNIQUENESS OF RESPONSE

We should distinguish between uniqueness of the constitutive equation and uniqueness of the solution of a boundary value problem (BVP).

3.1 | Constitutive uniqueness

'Controllability' is a constitutive property of a material, i.e. a property of its constitutive relation. Considering the six independent components of the stretching tensor $\mathbf{D}$ and the corresponding ones of the stress rate $\mathring{\mathbf{T}}$, controllability in the sense of Nova[10] means that a partition of six components of either the $\mathbf{D}$ or $\mathring{\mathbf{T}}$ - tensors (such that all of them have different indices) uniquely defines the complementary components. Positive second order work implies controllability in this sense but not homogeneity of stress and strain in a laboratory test.

3.2 | Uniqueness of the solution of a BVP

An affine deformation within a sample whose boundary undergoes an affine motion $\mathbf{v}(\mathbf{x}_{\text{boundary}}) = \mathbf{A}\mathbf{x}_{\text{boundary}}$ with $\mathbf{A}$ = const can be obtained subject to the condition expressed by Eq. 4. Clearly, the affine motion $\mathbf{v} = \mathbf{A}\mathbf{x}$ is a solution of the boundary value problem, if we neglect gravity. We consider whether this solution is unique. Assume that there exists also another solution $\bar{\mathbf{v}} \neq \mathbf{v}$. Denoting differences by the symbol Δ, e.g. $\Delta\mathbf{v} = \mathbf{v} - \bar{\mathbf{v}}$, we observe that $\Delta\mathbf{v}$ vanishes at the boundary. The equilibrium equation reads $\nabla \cdot \mathbf{T} = \mathbf{0}$, and continued equilibrium reads $\nabla \cdot \dot{\mathbf{T}} = \mathbf{0}$. The same equations hold also for the stress difference $\Delta\mathbf{T} := \mathbf{T} - \bar{\mathbf{T}}$: $\nabla \cdot \Delta\mathbf{T} = \mathbf{0}$ and $\nabla \cdot \Delta\dot{\mathbf{T}} = \mathbf{0}$. Now we consider the integral $I := \int_V \nabla \cdot (\Delta\dot{\mathbf{T}}\Delta\mathbf{v})dV$ and apply the theorem of GAUSS. We thus obtain, that this integral vanishes:

$$\int_V \nabla \cdot (\Delta\dot{\mathbf{T}}\Delta\mathbf{v}) \, dV = \int_S \left(\Delta\dot{\mathbf{T}}\Delta\mathbf{v}\right) \cdot \mathbf{n} \, dS = 0, \tag{1}$$

because $\Delta\mathbf{v} = \mathbf{0}$ on the surface S. Further,

$$I = \int_V \nabla \cdot (\Delta\dot{\mathbf{T}}\Delta\mathbf{v}) \, dV = \int_V \Delta\dot{\mathbf{T}} \cdot (\nabla \cdot \Delta\mathbf{v}) \, dV + \int_V \Delta\mathbf{v} \cdot \left(\nabla \cdot \Delta\dot{\mathbf{T}}\right) \, dV = 0. \tag{2}$$

The second integral on the right hand side vanishes due to continued equilibrium. Thus, for non-uniqueness the following statement must hold:

$$\int_V \Delta\dot{\mathbf{T}}\cdot(\nabla\Delta\mathbf{v})\,dV = \int_V \Delta\dot{\mathbf{T}}\cdot\Delta\mathbf{L}\,dV = \int_V \Delta\dot{\mathbf{T}}\cdot\Delta\mathbf{D}\,dV = 0, \tag{3}$$

which is impossible if $\Delta\dot{\mathbf{T}}\cdot\Delta\mathbf{D} > 0$ holds everywhere. Note that $\mathbf{L} := \nabla\mathbf{v} = \mathbf{D}+\mathbf{W}$ with $\mathbf{D} = (\mathbf{L}+\mathbf{L}^{\mathsf{T}})/2$ and hence, $\dot{\mathbf{T}}\cdot\mathbf{L} = \dot{\mathbf{T}}\cdot\mathbf{D}$. Referring to tensors $\mathbf{X}$ and $\mathbf{Y}$ and vectors $\mathbf{x}$ and $\mathbf{y}$ we use the following notation: $\mathbf{xy} = x_i y_j$, $\mathbf{Xx} = X_{ik}x_k$, $\mathbf{X}\cdot\mathbf{Y} = X_{ik}Y_{ki}$, thus $\Delta\dot{\mathbf{T}}\cdot\Delta\mathbf{D}$ denotes the same as $\mathrm{tr}(\Delta\dot{\mathbf{T}}\Delta\mathbf{D})$. Hence the condition,

$$\mathrm{tr}(\Delta\dot{\mathbf{T}}\Delta\mathbf{D}) > 0, \tag{4}$$

implies uniqueness. For the special case $\bar{\mathbf{v}} = \mathbf{0}$ we have: $\mathrm{tr}(\Delta\dot{\mathbf{T}}\Delta\mathbf{D}) = \mathrm{tr}(\dot{\mathbf{T}}\mathbf{D})$. Hence, $\mathrm{tr}(\Delta\dot{\mathbf{T}}\Delta\mathbf{D}) > 0$ implies positive second order work: $\mathrm{tr}(\dot{\mathbf{T}}\mathbf{D}) > 0$, but the latter condition does not imply uniqueness.

Consider for example the oedometric test (Fig. 1) whose boundary conditions are kinematic. It is generally assumed that the deformation of a sand sample in the oedometer is homogeneous. However, this is not necessary, as already mentioned, as the tangential velocity along the walls is not prescribed.
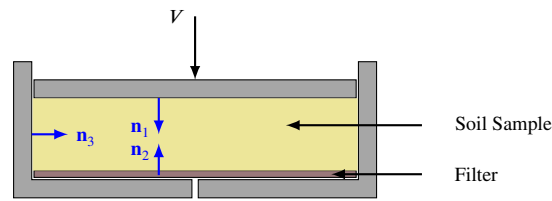

FIGURE 1 Schematic illustration of the oedometric test

We decompose the velocity $\mathbf{v}$ into the mean velocity $\bar{\mathbf{v}}$ and its fluctuation $\mathbf{v}'$:

$$\mathbf{v} = \bar{\mathbf{v}} + \mathbf{v}'. \tag{5}$$

With $\mathbf{n}_1, \mathbf{n}_2, \mathbf{n}_3$ being the unit normal vectors at the upper and lower plates and the side wall (see Fig. 1), respectively, the boundary conditions read:

$$\mathbf{v}\cdot\mathbf{n}_1 = \bar{\mathbf{v}}\cdot\mathbf{n}_1 = V, \quad \mathbf{v}'\cdot\mathbf{n}_1 = 0, \tag{6}$$
$$\mathbf{v}\cdot\mathbf{n}_2 = \bar{\mathbf{v}}\cdot\mathbf{n}_2 = \mathbf{v}'\cdot\mathbf{n}_2 = 0 \tag{7}$$
$$\mathbf{v}\cdot\mathbf{n}_3 = \bar{\mathbf{v}}\cdot\mathbf{n}_3 = \mathbf{v}'\cdot\mathbf{n}_3 = 0, \tag{8}$$
$$\tag{9}$$

where V is the vertical velocity of the piston. Consequently, the velocity fluctuation $\mathbf{v}'$ is tangential to all boundaries. According to a theorem by Kelvin and Helmholtz on the impossibility of irrotational motions in general (cited by Truesdell[11], section 37), the field $\mathbf{v}'$ is in this case either rotational or zero. The latter case corresponds to the homogeneous deformation, which is of course possible.

4 | VORTICES OBTAINED WITH THE MESHLESS CODE SPARC

The meshless code SPARC uses constitutive relations from the realm of continuum mechanics, in particular the barodetic[12] constitutive relation. No Cosserat effects are considered. It is interesting to note that SPARC simulations automatically reveal vortices in the velocity fluctuations.

For completeness, the basics of the code are outlined here and its framework is summarized in Fig. 2 . For further details on the development and applications of the code SPARC, refer to [13,14,15,16,17].

Discretization: The continuum is represented by m material points. At a time t each material point is assigned position $\mathbf{x}$, velocity $\mathbf{v}$, density ρ (or void ratio e) and stress $\mathbf{T}$.

Governing equation: Quasistatic equilibrium prevails at each material point, i.e. the CAUCHY equation $\mathrm{div}\mathbf{T} + \rho\mathbf{g} = \mathbf{0}$ holds.
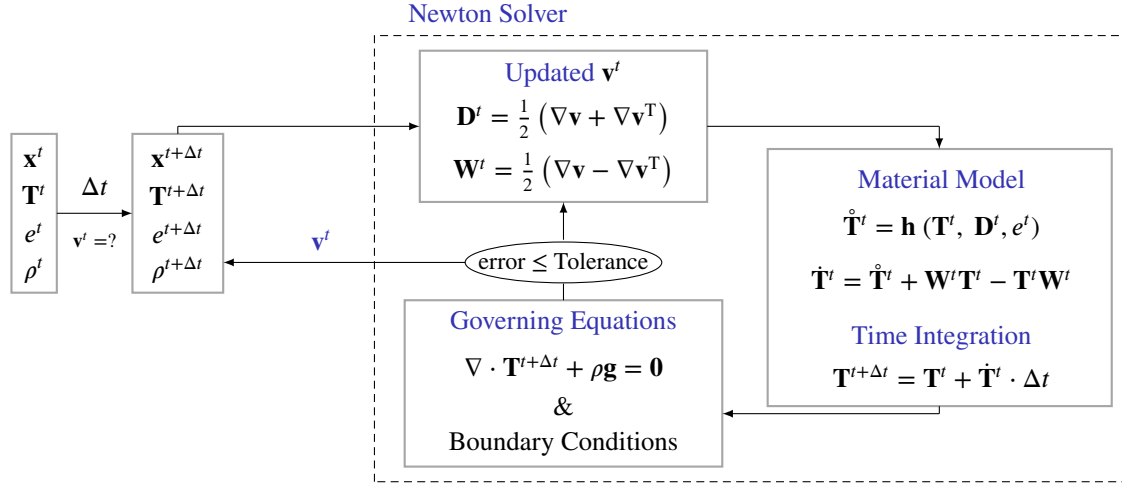
FIGURE 2 Framework of SPARC

To numerically evaluate this equation, the spatial derivatives in the term div**T** are obtained by interpolation/approximation of **T** based on the neighbor points. Fulfillment of the equilibrium equation means *strong solution* at the selected mass points *(collocation)*.

Time integration: The stress at the next time step is obtained with, say, an Euler-forward scheme as $\mathbf{T}^{t+\Delta t} = \mathbf{T}^t + \dot{\mathbf{T}}^{t+\Delta t} \cdot \Delta t$. The stress rate $\dot{\mathbf{T}}^{t+\Delta t}$ is obtained by means of a given constitutive equation, $\dot{\mathbf{T}} = \mathbf{h}(\mathbf{T}, \mathbf{D}, e)$, where the stretching **D** is obtained from the spatial derivatives of the velocity field. Again, these derivatives are obtained by interpolation/approximation of the velocity field based on the velocities $\mathbf{v}^{t+\Delta t}$ of the considered mass point and its nearest neighbors. These velocities are iteratively obtained with a Newton scheme so as to fulfil the equations of equilibrium at the time $t + \Delta t$.

Ordinary FEM simulations typically use the weak form of equilibrium. Hence, the underlying integration implies smoothing and, therefore, vortices usually do not appear. SPARC uses strong equilibrium and, thus, avoiding smoothing is capable to show vortices.

4.1 | Barodetic material model

We use for the simulations in this study the constitutive model of barodesy [18]. This model is rate-independent and yields an evolution equation for the CAUCHY stress tensor **T**: The co-rotated stress rate $\mathring{\mathbf{T}}$ is expressed as a function of the current stress state **T**, the stretching tensor **D** and the void ratio e,

$$\mathring{\mathbf{T}} = \mathbf{h}(\mathbf{T}, \mathbf{D}, e). \tag{10}$$

The barodetic model for sand reads [1],

$$\mathring{\mathbf{T}} = h(\mathbf{T}) \cdot \left(f \mathbf{R}^0 + g \mathbf{T}^0 \right) \cdot |\mathbf{D}|, \tag{11}$$

where,

$$h = -\frac{c_4 + c_5 |\mathbf{T}|}{e - e_{\min}} \tag{12}$$

$$f = \operatorname{tr} \mathbf{D}^0 + c_3 e_c, \quad g = -c_3 e \tag{13}$$

$$\mathbf{R} = -\exp\left[c_1 \exp\left(c_2 \cdot \operatorname{tr} \mathbf{D}^0 \right) \mathbf{D}^0 \right] \tag{14}$$

$$e_c = \frac{e_{\min} + B}{1 - B}, \quad B = \frac{e_{c0} - e_{\min}}{e_{c0} + 1} \left(\frac{c_4 + c_5 \cdot |\mathbf{T}|}{c_4} \right)^{-(1+e_{\min})/c_5} \tag{15}$$

---

[1] $|\mathbf{X}| = \sqrt{\operatorname{tr}(\mathbf{X}^2)}$ and $\mathbf{X}^0 = \mathbf{X}/|\mathbf{X}|$
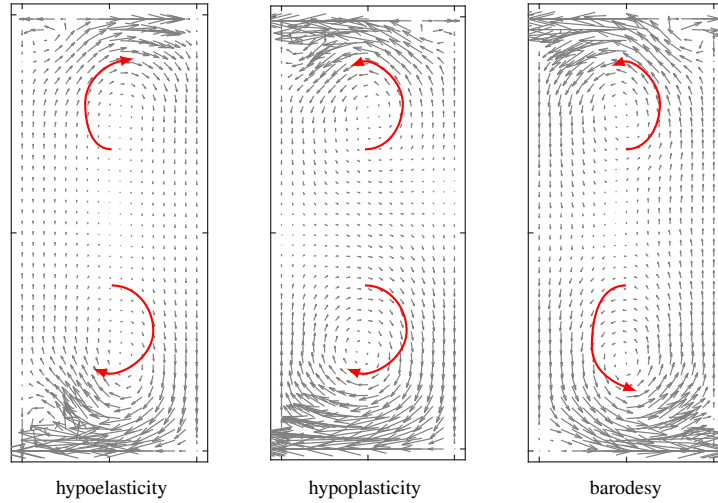
FIGURE 3 Comparison of formation of vortices in an oedometric test obtained with SPARC with three different material models

Eq. 11 is positively homogeneous of the first degree in $\mathbf{D}$, which implies rate-independent behavior of the material.
For the simulations in this study, we use the calibration of barodesy for Hostun-sand with critical friction angle $\varphi_c = 33.8°$, $e_{min} = 0.63$, $e_{max} = 1$ and $D_{50} = 0.35$ mm. The used material constants are summarized in Tab. 1 . A barodetic model for clay has been presented by Medicus and Fellin [19].

c_1	c_2	c_3	c_4	c_5	e_{c0}	e_{min}
-1.0246	1	-2.3	465	28	0.87	0.35

TABLE 1 Material constants for Hostun sand [18]

5 | NUMERICAL SIMULATION OF VORTICES WITH SPARC

Firstly, the oedometric test is chosen for our demonstrations, because it is generally believed that this test has a homogeneous (affine) deformation, whereas we prove here that this is not necessarily the case. In our numerical simulations we consider lengthy oedometric samples, which are unusual, because the vortices, the diameter of which depends on the dimensions of the container, are there more pronounced.
In order to demonstrate that the formation of vortices is independent of the applied material model, firstly a comparison of an oedometric test with smooth upper and lower plates with three different material models is shown in Fig. 3 . The three material models are, (i) hypoelastic (i.e. $\dot{\mathbf{T}} = \lambda \operatorname{tr} \mathbf{D} \mathbf{1} + 2\mu\mathbf{D} + \mathbf{WT} - \mathbf{TW}$ with $\lambda = 266.67$ MPa and $\mu = 400$ MPa), (ii) hypoplastic material model after VON WOLFFERSDORFF [20] and (iii) barodesy for sand after KOLYMBAS (2015) [18], introduced in Sec.4.1. The results show that regardless of the selected material model, the vortices follow almost the same pattern. We consider now oedometric, biaxial and simple shear tests simulated with the barodetic material model after KOLYMBAS (2015) [18]. The stress-strain relations of oedometer, true biaxial and simple shear tests with the above mentioned material model are shown in Fig. 4 . In Fig. 5 we show the development of vortices with increasing deformation in an oedometric test with rough upper and lower plates. No particular pattern of the vortices can be detected and the vortices look different with increasing ε_{zz}. Since Fig. 5 - f, gives the impression of non-vanishing velocity-fluctuations adjacent and normal to the upper plate, a zoom of this figure at the upper plate is plotted in Fig. 6 .
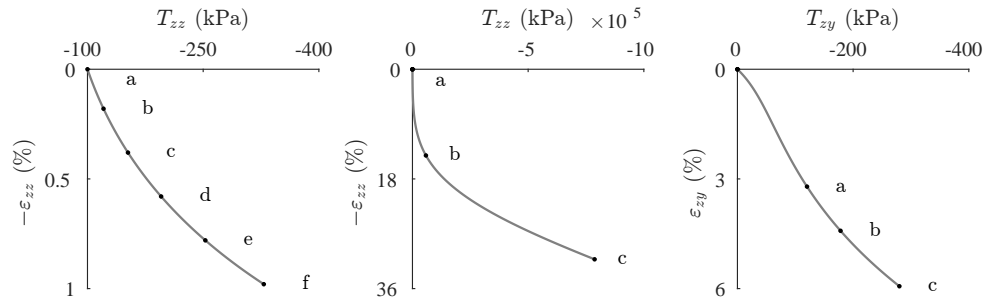
FIGURE 4 Stress-strain curves for oedometer (left), true biaxial (middle) and simple shear simulations (right), recpectively
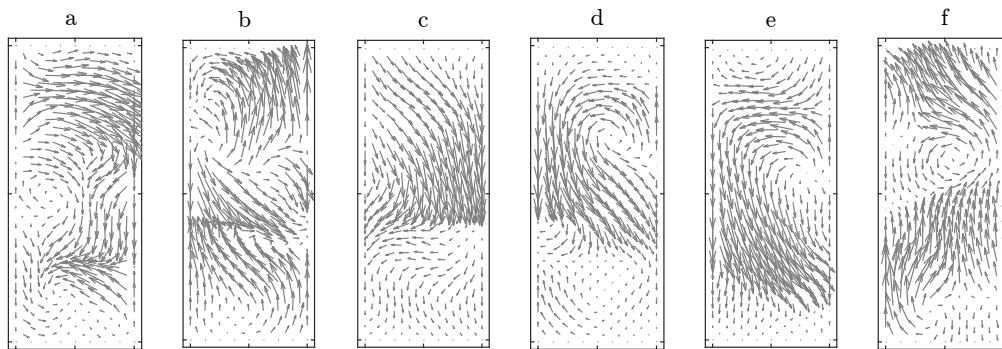

FIGURE 5 Development of vortices with increasing oedometric deformation, at the strains indicated in Fig. 4 - left, *rough* upper and lower plates. Fig. f gives the impression of non-vanishing normal fluctuations adjacent to the upper plate. Therefore, a zoom is plotted in Fig. 6
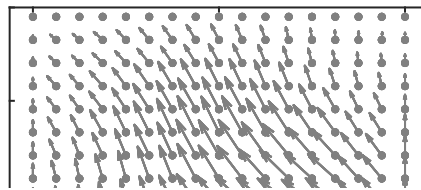

FIGURE 6 Zoom of Fig 5 - f.

In Fig. 7 the development of vortices with increasing deformation in an oedometric test with smooth upper and lower plates is plotted. In contrast to Fig. 5 an almost constant pattern of vortices can be detected in this case. The vortices are mainly formed at the upper and lower plates with a rotational pattern.

In Fig. 8 the effect of the dimension of the model on the vortices in an oedometric test with rough upper and lower plates is shown.

In Fig. 9 the influence of the number of the particles on the vortices is shown. It can be seen that for larger spacing d (fewer number of particles) the vortices can still be detected. However the vortices have a simpler pattern, and as the spacing d gets smaller and the number of particles increases, the vortices become more complex.

In Fig. 10 the development of vortices is shown with increasing deformation in a true biaxial test. At the beginning of the deformation, Fig. 10 - a, the vortices show a simple pattern of rotation. With increasing deformation, the vortices form an almost symmetrical pattern with rotations in opposite directions.

In Fig. 11 the development of vortices with increasing deformation in a simple shear test is shown. In Fig. 11 - a, at the beginning of the deformation, the vortices show a rotational pattern. However with increasing deformation, the rotational pattern of vortices disappears and the vortices move to the top left of the model. A more comprehensive parameter study on the formation of vortices with SPARC is presented by Bathaeian[13].
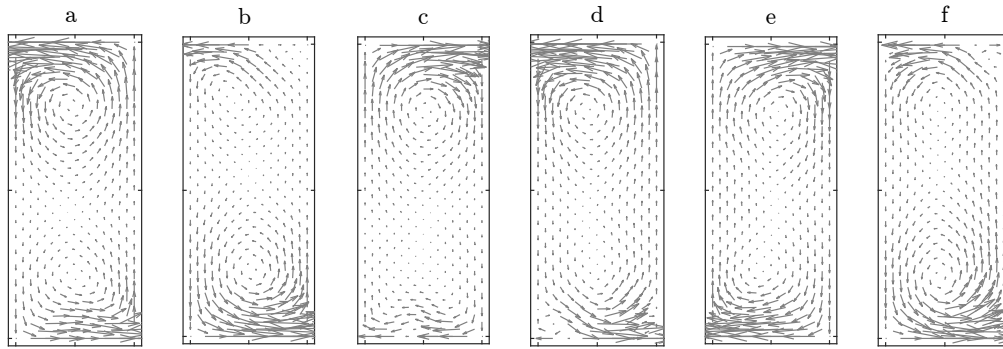
FIGURE 7 Development of vortices with increasing oedometric deformation, at the strains indicated in Fig. 4 - with *smooth* upper and lower plates. The cases a to f correspond to cases a to f in Fig. 4 .
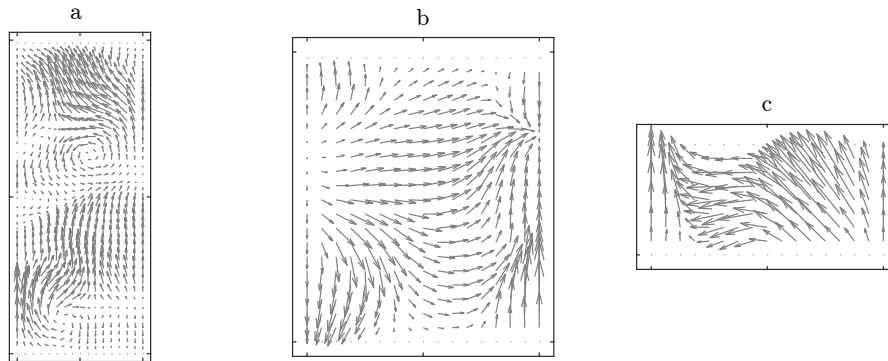

FIGURE 8 Influence of the sample size on oedometric deformation, a) $h_0/B = 2.5$, b) $h_0/B = 1.25$ and c) $h_0/B = 0.5$ - rough upper and lower plates
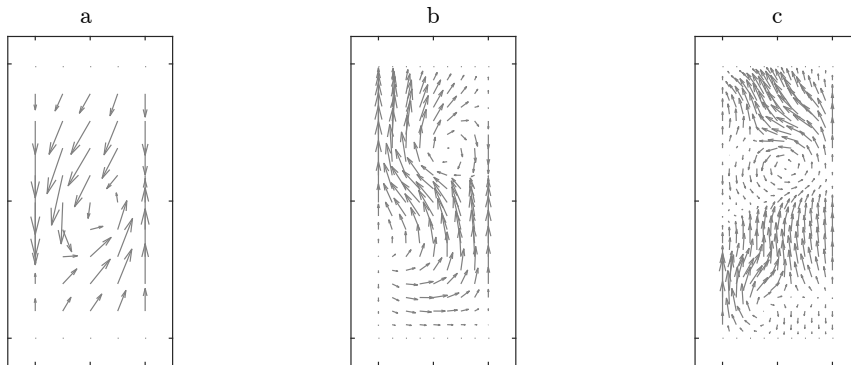

FIGURE 9 Influence of the density of particles (initial spacing size d in the oedometric test simulation) a) $d = 50$ mm, b) $d = 25$ mm and c) $d = 12.5$ mm - rough upper and lower plates
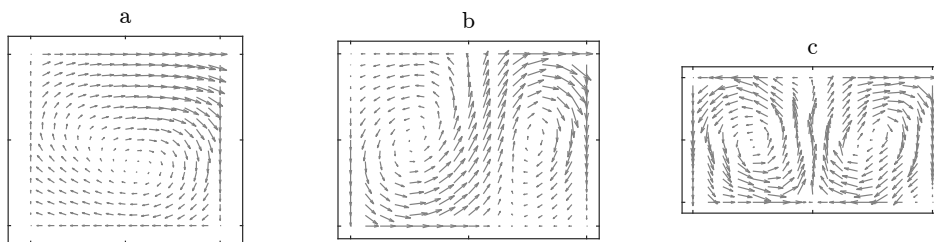

FIGURE 10 Development of vortices with increasing biaxial deformation at the strains indicated in Fig. 4 - middle
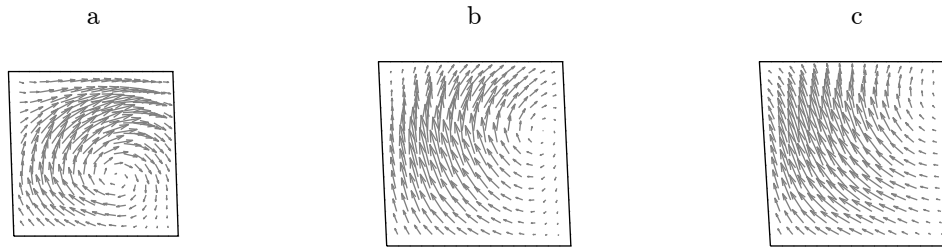
FIGURE 11 Development of vortices with increasing simple shear deformation at the strains indicated in Fig. 4   - right

6 | PHYSICAL JUSTIFICATION OF VORTICES

Although vortices in granular motion have been observed in physical experiments and numerical simulations of various types, their physical explanation is still speculative. Shear motion in a contractant granular body reduces the hydrostatic stress and, hence, reduces the overall stiffness. Thus, the superposition of vortices to an affine deformation implies a superimposed shear, and this reduces the volumetric stiffness and, consequently, also the overall stiffness of contractant media. In microscopic terms, the irreversible deformation of granulates is related to rearrangement of "rigid" grains, which can hardly occur with affine deformations. Thus, vortices may originate from grain re-arrangement, see also Tordesillas et al.[9]. Some authors, see e.g. Liu et al.[21] attribute the appearance of vortices to buckling of force chains. Interestingly, Cosserat rotations seem to inhibit rather than enforce the appearance of vortices, see Alonso-Marroquin et a.[22]

7 | IMPLICATIONS FOR ELEMENT TESTS

For an oedometric test, the stress-strain curve obtained from direct integration of the material model and assuming homogeneous deformation is compared with the one from SPARC, by which the stress is influenced by turbulence. The mean value of vertical normal stress T_{zz} for the simulation with turbulence is calculated as follows,

$$\bar{T}_{zz} = \frac{\int_{y_{\min}}^{y_{\max}} T_{zz} \cdot d y}{y_{\max} - y_{\min}} \tag{16}$$

where $y_{\min}$ and $y_{\max}$ represent the horizontal boundaries of the model. In Fig. 12 , δ demonstrates the difference in the vertical stresses T_{zz}, with and without vortices. Obviously, this difference is very small.

8 | PTYGMATIC FOLDS

Ptygmatic folds are a peculiar pattern of folding in rock, see Fig. 13 . The general assumption in geology is that ptygmatic folds occur when a sheet of stiffer rock (termed as "competent") is confined by a softer host material and undergoes plastic deformation, according to Godfrey[23]. Here we show that ptygmatic folds can be a consequence of turbulent deformation of geomaterials.

8.1 | Simulation of ptygmatic folds with SPARC

It is a striking fact that deformation of rock can, in many cases, be modelled, with constitutive relations for soils, i.e. materials with no or low cohesion. Thus, modelling of rock folding in the laboratory can be investigated with dry sand (so-called sandbox models, see e.g. Panien et al.[24]). To name a few more, the reader is referred to the experiments of Cloos[25] using clay for modelling patterns in geology and the models developed by Budd et al[26], Ramberg and Ove[27] for modelling deformations in geological strata.
For the simulation of the ptygmatic folds a simple shear test of a clay sample with initial height of 50 cm and width of 10 cm
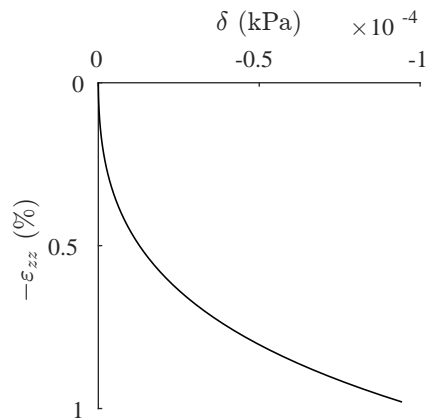
FIGURE 12 Effect of turbulences on the stress-strain relation - development of difference in T_{zz} (with and without vortices) with increasing oedometric deformation
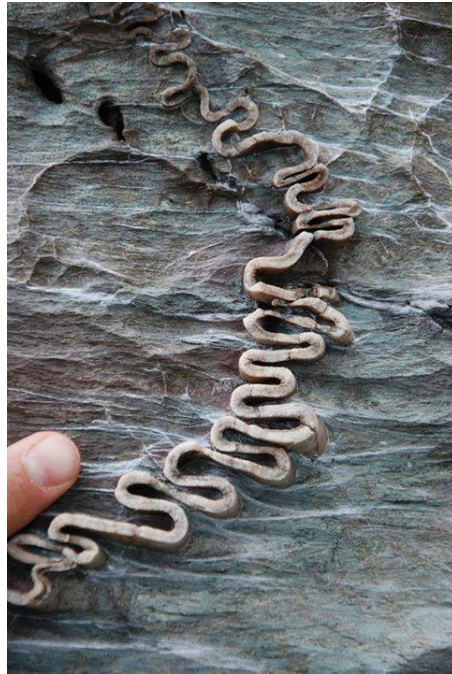

FIGURE 13 Ptygmatic folds in rock, Photo from: Rodolfo Carosi, University of Torino, Outcropedia, reprinted with permission

under plane strain has been simulated (see Fig. 14). The void ratio of the red particles on the material line $y = 0.05$ m has been reduced by 20% in comparison to the void ratio of the gray particles. The lower void ratio for the red particles leads to a more competent behavior of the material line ($y = 0.05$ m) in comparison to the host gray particles. A homogeneous setup is also simulated, by which all particles have the same initial void ratio. The simulation is repeated for a homogeneous setup in order to investigate whether the appearance of ptygmatic folds is due to the presence of a competent material confined by less competent host material or not.
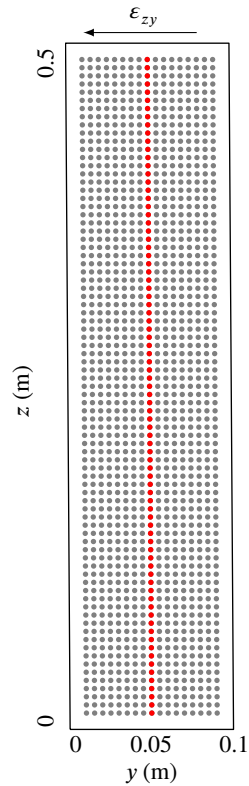
FIGURE 14 Geometry of the model, the red particles in the middle of the model represent the "competent material line" with reduced void ratio of $\Delta e = 20\ \%$
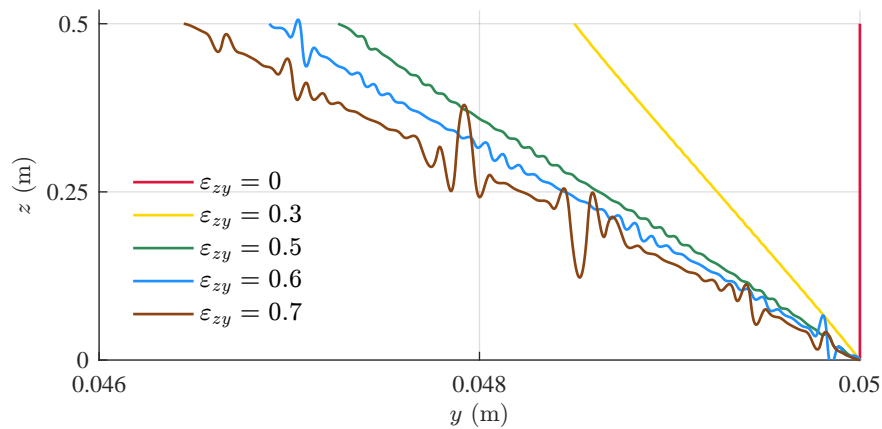

FIGURE 15 Deformation of the material line ($y = 0.05$ m) in simple shear tests for set-up with competent material

8.1.1 | Results

The deformation of the material line ($y = 0.05$ m line in Fig. 14) with increasing shear strain (ε_{zy}) is plotted in Fig. 15 . The material shows minute folds at $\varepsilon_{zy} = 0.3$. However as the sample is sheared further, the ptygmatic folds along the material line become more apparent until for $\varepsilon_{zy} = 0.7$ the fold becomes significant.

 In Fig. 16 , the deformation of the material line ($y = 0.05$ m) for homogeneous set-up and increasing shear strain is plotted. In contrast to Fig. 15 , no folds can be detected along the material line which keeps its initial form throughout the simulation.
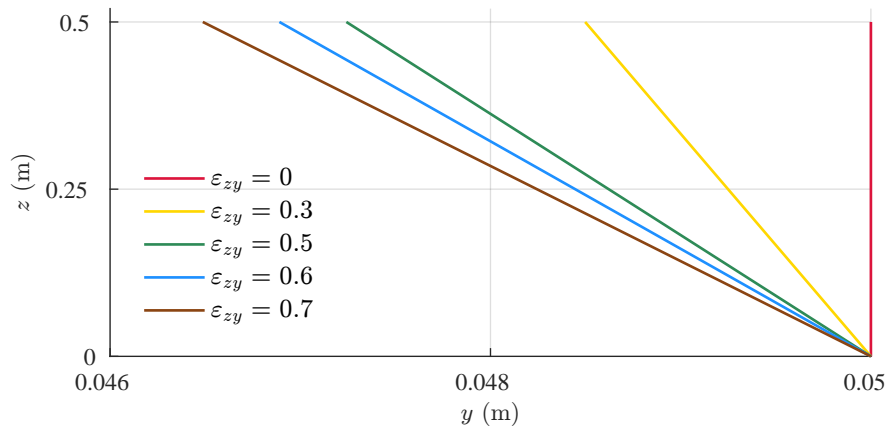
FIGURE 16 Deformation of material line ($y = 0.05$ m) in simple shear test for homogeneous set-up

In Fig. 17 , the vortices at $\varepsilon_{zy} = 0.7$ are compared for the simulation with homogeneous set-up and the simulation with the competent material line. The vortices differ clearly from each other and in case of the set-up with the competent material line, the vortices are in correspondence with the deformed material line in Fig. 15 .

The question arises why no ptygmatic folds can be detected in Fig. 16 , although vortices for the homogeneous set-up (Fig. 17 , left) are detectable. This question can be answered by investigating the intensity of vortices. In Fig. 18 , the norm of velocity fluctuation, $|\mathbf{v}'|$, is plotted for different variations in the void ratio of the competent material line, where $\Delta e = 0$ represents the homogeneous set-up. As it can be seen, for $\Delta e = 0$, the norm of fluctuation becomes very small ($|\mathbf{v}'| = 1.5 \times 10^{-13}$ m/s) and with increasing Δe, the intensity of fluctuation becomes 4×10^9 times larger and reaches $|\mathbf{v}'| = 6 \times 10^{-4}$ m/s.

9 | CONCLUSION

Vortices have been observed with DIC in laboratory tests and in DEM simulations of deformations of granular bodies. In this paper we present a simulation of vortices based on a numerical solution of problems formulated in terms of continuum mechanics. Our results can be applied to the interpretation of laboratory tests with soil and other granular materials. Such tests are often expected to be element tests, and experimentators are often surprised to realize that several patterns of inhomogeneous deformation set on. We also point to the possible applicability of our findings to structural geology.
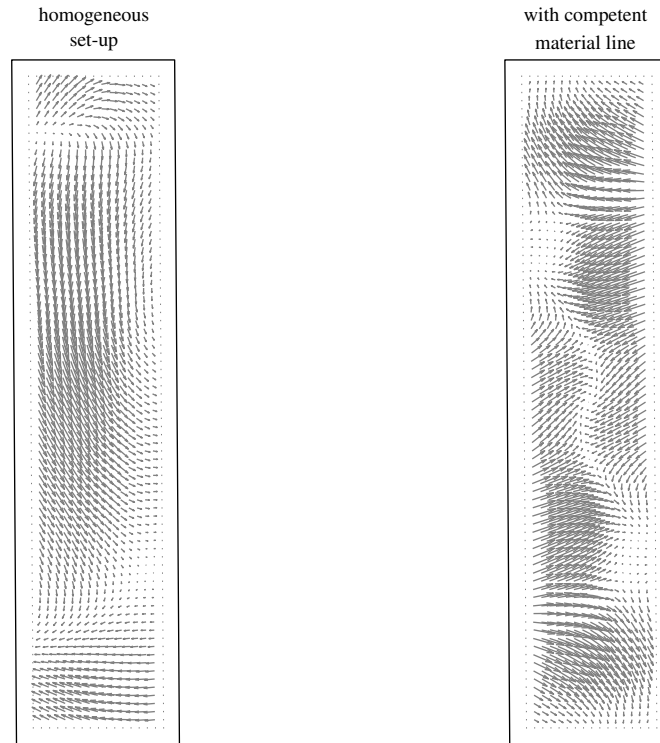
FIGURE 17 Comparison of vortices in a simple shear test for homogeneous set-up (left) and set-up with competent material line (right), $\varepsilon_{zy} = 0.7$
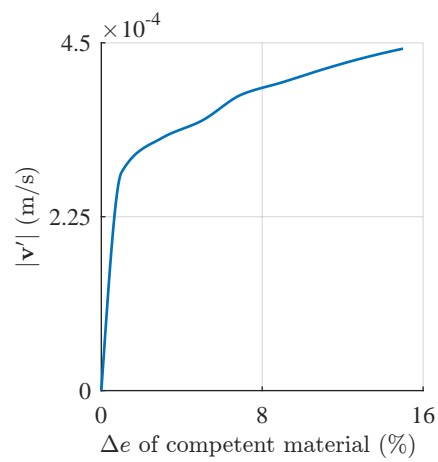

FIGURE 18 Fluctuation ($\mathbf{v}'$) in dependence of void ratio of the competent material line, $\Delta e = 0$ % represents the homogeneous set-up and $\Delta e = 16$ % means $e_0 = 0.425$ for the competent material line

10 | ACKNOWLEDGEMENT

References

1. Abedi Sara, Rechenmacher Amy L., Orlando Andrés D. Vortex formation and dissolution in sheared sands. *Granular Matter.* 2012;14(6):695–705.

2. Richefeu V., Combe G., Viggiani G. An experimental assessment of displacement fluctuations in a 2D granular material subjected to shear. *Géotechnique Letters.* 2012;2(3):113-118.

3. Thornton C., Zhang L. A numerical examination of shear banding and simple shear non-coaxial flow rules. *Philosophical Magazine.* 2006;86(21-22):3425–3452.

4. Kozicki Jan, Niedostatkiewicz Maciej, Tejchman J., Muhlhaus H-B. Discrete modelling results of a direct shear test for granular materials versus FE results. *Granular Matter.* 2013;15(5):607–627.

5. O'Donovan J., O'Sullivan C., Marketos G. Two-dimensional discrete element modelling of bender element tests on an idealised granular material. *Granular Matter.* 2012;14(6):733–747.

6. Peters John F, Walizer Laura E. Patterned nonaffine motion in granular media. *Journal of Engineering Mechanics.* 2013;139(10):1479–1490.

7. Revuzhenko A. F. Odnorodnaya deformatsiya splochnoy sredy. *Prikladnaya Mekhanica i tekhnicheskaya Fysika.* 1997;38(3).

8. Desrues J., Andò E., Bésuelle P., et al. Localisation Precursors in Geomaterials. In: Papamichos Euripides, Papanastasiou Panos, Pasternak Elena, Dyskin Arcady, eds. *Bifurcation and Degradation of Geomaterials with Engineering Applications. IWBDG 2017*, :3–10, Springer International Publishing; 2017.

9. Tordesillas Antoinette, Pucilowski Sebastian, Walker David M., Peters John F., Walizer Laura E.. Micromechanics of vortices in granular media: connection to shear bands and implications for continuum modelling of failure in geomaterials. *International Journal for Numerical and Analytical Methods in Geomechanics.* 2014;38(12):1247–1275.

10. Nova Roberto. Controllability of the incremental response of soil specimens subjected to arbitrary loading programmes. *Journal of the Mechanical behavior of Materials.* 1994;5(2):193–202.

11. Truesdell Clifford. *The kinematics of vorticity.* Indiana University Press, Bloomington; 1954.

12. Kolymbas D. Barodesy: a new Hypoplastic approach. *International Journal for Numerical and Analytical Methods in Geomechanics.* 2011;36(9):1220-1240.

13. Bathaeian I. Meshfree Simulation of Problems in Soil Mechanics, Laboratory Tests - Shear Bands - Punching - Cone Penetration - Turbulence in Granular Solids - Ptygmatic Folds. PhD thesis, University of Innsbruck, Unit of Geotechnical and Tunnel Engineering, 2018.

14. Chen Chien-Hsun. *Development of Soft Particle Code (SPARC).* Advances in Geotechnical Engineering and Tunnelling, Logos Verlag Berlin GmbH; 2015.

15. Polymerou Iliana. *Untersuchung großer Verformungen in der Vertushka.* Advances in Geotechnical Engineering and Tunnelling, Logos Verlag Berlin GmbH; 2017.

16. Michel I., Bathaeian S. M. I., Kuhnert J., et al. Meshfree generalized finite difference methods in soil mechanics—part II: numerical results. *GEM - International Journal on Geomathematics.* 2017;8(2):191–217.

17. Schneider-Muntau Barbara, Chen Chien-Hsun, Bathaeian S. M. Iman. Simulation of shear bands with Soft PARticle Code (SPARC) and FE. *GEM - International Journal on Geomathematics.* 2017;8(1):135–151.

18. Kolymbas D. Introduction to Barodesy. *Géotechnique.* 2015;65(1):52-65.

19. Medicus Gertraud, Fellin Wolfgang. An improved version of barodesy for clay. *Acta Geotechnica.* 2017;12(2):365–376.

20. von Wolffersdorff P.-A. A Hypoplastic Relation for Granular Materials with a Predefined Limit State Surface. *Mechanics of Cohesive-Frictional Materials.* 1996;1:251-271.

21. Liu Xiaoxing, Papon Aurélie, Muhlhaus Hans. Numerical study of structural evolution in shear band. *Philosophical Magazine.* 2012;92(28-30):3501–3519.

22. Alonso-Marroquin F, Vardoulakis I, Herrmann Hans Jürgen, Weatherley D, Mora P. Effect of rolling on dissipation in fault gouges. *Physical Review E.* 2006;74(3):031306.

23. Godfrey John D. The origin of ptygmatic structures. *The Journal of Geology.* 1954;62(4):375–387.

24. Panien Marion, Schreurs Guido, Pfiffner Adrian. Sandbox experiments on basin inversion: testing the influence of basin orientation and basin fill. *Journal of Structural Geology.* 2005;27(3):433–445.

25. Cloos Hans. Hebung-Spaltung-Vulkanismus, Elemente einer geometrischen Analyse irdischer Grossformen. *Geol. Rund..* 1939;30:406–527.

26. Budd Chris J, Hunt Giles W, Peletier Mark A. Self-similar fold evolution under prescribed end-shortening. *Mathematical geology.* 1999;31(8):989–1005.

27. Ramberg Hans, Stephansson Ove. Compression of floating elastic and viscous plates affected by gravity, a basis for discussing crustal buckling. *Tectonophysics.* 1964;1(1):101–120.

How to cite this article: Kolymbas D., and Bathaeian I. (2018), Numerically obtained vortices in granular media, *International Journal for Numerical and Analytical Methods in Geomechanics*, .